The International Journal of Advanced Manufacturing Technology
https://doi.org/10.1007/s00170-020-06585-z

ORIGINAL ARTICLE

Performance evaluation of the edge preparation of tungsten carbide inserts applied to hard turning

Carlos E. H. Ventura[1] · Frederico C. Magalhães[2] · Alexandre M. Abrão[2] · Berend Denkena[3] · Bernd Breidenstein[3]

Received: 28 September 2020 / Accepted: 30 December 2020

Abstract
Owing to their inferior hot hardness in comparison with alumina-based ceramics and polycrystalline cubic boron nitride, the performance of coated carbide tools when turning hardened steels strongly relies on proper chemical composition and carbide grain size, together with adequate cutting edge preparation. This work investigates the effect of geometric parameters on the performance of cutting tools applied to turning of AISI 4140 steel hardened to 40 and 50 HRC, in terms of the components of the turning force and temperature. Additionally to well-established geometric parameters, such as the projection of the hone radius on the rake face (S_γ), the projection of the hone radius on the clearance face (S_α), and the form factor K (ratio of S_γ to S_α), a novel parameter is proposed, namely perimeter ratio (P), which represents the ratio of the perimeter of the modified cutting edge to the circumference of the standard honed edge. Moreover, the experimental results were compared with analytical and numerical findings in order to assess their effectiveness in predicting the components of the turning force and chip temperature. The results indicated that analytical modeling was capable to satisfactorily predict the variation of the force components with edge preparation, using as input the value of the corresponding experimental forces for the standard honed cutting edge. On the other hand, the numerical modeling was successfully applied to predict the components of the resultant force at the expense of higher computational effort. The cutting force was not drastically affected by edge preparation, whereas the feed and passive forces increased with P and S_α and the form factor K was not capable to provide a consistent relationship with both the feed and passive forces. Both the experimental and numerical temperatures of the chip and the numerical temperature at the tool-chip interface did not present a straightforward trend with regard to edge preparation.

Keywords Cutting edge preparation · Turning · Forces · Temperature · Numerical simulation · Hardened steel

1 Introduction

During hard part machining, the cutting tool is subjected to severe thermal and mechanical loading, which may lead to either progressive wear at accelerated rates or catastrophic failure. Therefore, monitoring the process forces and temperature plays a key role with regard to both technical (thermal damage to the component, quality of the machined surface, etc.) and economic (tool costs) aspects. For instance, the machined surface roughness is expected to decrease when the work material hardness is elevated; however, the corresponding elevation of the process force components may lead to tool, holder, and/or workpiece deflection as well as vibrations that may impair dimensional and geometric accuracy.

The influence of workpiece hardness on the performance of machining operations is not straightforward. Lima et al. [1] noticed that the cutting force decreased slightly when the hardness of AISI 4340 steel was increased from 250 to 345 HV, but increased with a further elevation to 415 HV, while the feed and thrust forces increased steadily with workpiece hardness. This behavior, also reported by Matsumoto et al. [2], can be explained by the fact that the increase in the shear strength of the work material is counterbalanced by the smaller chip-tool contact area.

✉ Frederico C. Magalhães
fredmag@demec.ufmg.br

[1] Department of Mechanical Engineering, Federal University of São Carlos, Rodovia Washington Luís km 235, São Carlos, SP 13565-905, Brazil

[2] Universidade Federal de Minas Gerais, Av. Antônio Carlos, 6627, Pampulha, Belo Horizonte, MG 30270-901, Brazil

[3] Institute of Production Engineering and Machine Tools, Leibniz Universität Hannover, An der Universität 2, 30823 Garbsen, Germany

Published online: 19 January 2021

Although polycrystalline cubic boron nitride (PcBN) tools are the first choice for heavy and interrupted cutting of ferrous alloys with hardness above 50 HRC, Al_2O_3-based ceramics are a competing alternative for continuous finish of these materials, whereas more recently developed grades of cemented carbide are capable of tackling steels with hardness below 50 HRC when subjected to light cutting conditions. Furthermore, the advances in the technology devoted to cutting edge geometry preparation have allowed the expansion and overlap of the work material and operation ranges covered by the abovementioned cutting tool grades.

With the development of techniques such as brushing [3], laser ablation [4], magneto abrasive machining [5], electrical discharge machining [6], and grinding of discretized edge rounding [7], cutting edge preparation with tailored geometries has become available to suit specific applications, in opposition to off the shelf-honed, chamfered (single or double), or a combination of honed and chamfered edges. Nevertheless, Denkena et al. [8] state that the hone radius alone is not sufficient to precisely characterize different cutting edge geometries and add the form factor K, defined as the ratio of S_γ (projection of the hone radius on the rake face of a virtually sharp cutting edge) to S_α (projection of the hone radius on the clearance face of a virtually sharp cutting edge). Thus, $K = 1$ represents a symmetrical cutting edge, while $K < 1$ indicates a slope toward the flank face and $K > 1$ a slope toward the rake face.

The performance of PcBN inserts with distinct microgeometries when turning hardened AISI 52100 bearing steel was investigated by Zhao et al. [9], who noticed that the smaller the hone radius, the larger the scatter around its nominal value in the same insert or in a set of inserts prepared with the same microgeometry. Moreover, the cutting tool with hone radius of $r_h = 20$ μm provided the lowest cutting force but largest flank wear, whereas the tool with $r_h = 30$ μm presented the best overall performance. Comparing the edge preparation of uncoated and coated carbide inserts, Ventura et al. [10] found better accuracy and narrower scatter for S_γ and S_α of the uncoated tools.

The performance of coated mixed alumina inserts with three distinct edge preparations (chamfered wiper inserts, chamfered and honed wiper inserts, and chamfered and honed conventional inserts) employed in turning of hardened AISI D2 steel was investigated by Khan et al. [11]. The findings indicated that tool life was not significantly affected by edge preparation; however, considerably lower surface roughness was provided by the wiper inserts, and the influence of edge preparation was negligible. Similar work was conducted by Souza et al. [12], who investigated the effect of edge preparation of PcBN inserts (honed against chamfered plus honed) on tool wear in orthogonal cutting of AISI M2 tool steel. The results indicated that the honed tools gave longest tool lives, while the chamfered and honed tools presented chipping on the rake face.

Owing to the high stresses and temperature gradients that take place in the tool-chip contact zone, a confined region and hardly accessible to transducers, the use of numerical modeling and simulation is essential for the better understanding of the behavior of these critical variables, which cannot be assessed experimentally. One must point out, however, that the majority of published work is concerned with orthogonal cutting; i.e., numerical modeling and simulation of three-dimensional cutting with emphasis on the cutting tool microgeometry are seldom reported.

Tiffe et al. [13] associated finite element modeling with statistical analysis in order to optimize the edge geometry of coated carbide drills used to cut Inconel 718. The experimental validation confirmed the proposed model; i.e., lowest wear was obtained for the optimized microgeometry with the hone radius shifted toward the clearance face, probably owing to the fact that tool temperature is lower in this case.

Finite element modeling was employed by Liao et al. [14] to predict the influence of the cutting tool rake angle and edge radius on chip deformation and stress applied to the tool during orthogonal cutting of a stainless steel. The rake angle ranged from 10 to 20° and the edge radius from 5 to 15 μm. The findings indicated that when the rake angle was elevated, the chip compression ratio decreased, and the stress applied to the tool increased, while the elevation of the edge radius had negligible influence on the chip compression ratio and its influence on the stress depended on the feed rate used.

The influence of hone radius and chamfer angle and width on chip formation, cutting forces, and temperature was studied by Yen et al. [15]. Finite element modeling of orthogonal cutting of AISI 1020 steel with uncoated tungsten carbide inserts was carried out, and the results compared with experimental data published previously. As far as the effect of edge honing is concerned, the cutting and thrust forces increased, and the shear angle decreased with the elevation of the edge radius due to the higher deformation required to shear the work material (a tenfold increase in the edge radius caused an increase in forces of 10 to 15%). The differences between numerical and experimental results (5–12% for the cutting force and 13–25% for the thrust force) were attributed to the large size of the workpiece elements at the tool tip compared to the very small edge radius, extrapolation errors regarding the material flow stress data at high strain rates and temperatures, and the simplified friction model used to represent the tool-chip interface. Moreover, the maximum interface temperature and both the normal and shear stress components were not affected by edge radius, while the average rake face temperature and the amount of plastic strain in the secondary shear zone increased with edge radius. With regard to the

influence of chamfer angle and width, their elevation resulted in higher temperatures as well as higher cutting and thrust forces, albeit the latter was more affected by chamfer angle (probably due to the increase in the effective tool-workpiece contact area).

Hua et al. [16] employed finite element modeling to predict the influence of cutting edge preparation on the magnitude and penetration depth of residual stresses induced by hard turning. Compressive residual stresses of higher intensity and reaching deeper beneath the surface were induced by turning with cutting tools possessing larger hone radius and tools with chamfered plus honed edge (in comparison with sharp edge, chamfered only, and honed edge with a smaller radius).

The application of tungsten carbide tools to turning of hardened steels has become feasible in more recent years only, thanks to the introduction of grades with submicrometric grain size and specific chemical composition. Despite such advances, tungsten carbide tools must be used under mild cutting conditions and to machine steels with moderately high hardness in order to avoid catastrophic failure or accelerated wear rates. Another relevant aspect to be considered in hard turning with tungsten carbide is cutting edge preparation, subject matter of the present work. Considering the influence of edge geometry on the mechanical and thermal loads imposed during machining and the fact that edge preparation plays a critical role on the performance of tungsten carbide inserts, whose mechanical properties (especially hot hardness) and chemical stability are inferior to PcBN and alumina-based ceramic tools, the aim of this work is to investigate the influence of a number of geometric parameters related to the cutting tool edge preparation on the process force components and temperature when hard turning AISI 4140 steel with coated tungsten carbide inserts.

The materials and experimental conditions employed in the present work are identical to those reported by Ventura et al. [10]; nevertheless, while the cited work was concerned with the influence of tool coating on the geometric parameters, the determination of the critical burnishing parameters and their influence on the cutting edge geometric parameters together with the influence of S_γ and S_α on the experimental turning force components, chip temperature, and machined surface roughness, the present work provides advances with regard to the mathematical treatment of the data. In addition to consolidated parameters, such as r_h, S_γ, S_α, and K, a new parameter named perimeter ratio P is proposed to overcome the drawback associated with the fact that the same form factor (K) will be obtained as long as the proportion between Sγ and Sα remains unaltered, irrespective of their magnitudes. Moreover, analytical and numerical models are employed to predict the behavior of the turning force components and chip temperature aiming to identify the geometric parameters and corresponding values associated with more efficient cutting.

2 Materials and methods

2.1 Experimental procedure

Cutting tool edge preparation was conducted on a KUKA KR16 robotic arm used to brush ISO grade H20 tungsten carbide inserts with geometry SNMN 120408 (cutting edge angle $\chi_r = 45°$, included angle $\varepsilon_r = 90°$, cutting edge inclination angle $\lambda_s = -5.5°$, rake angle $\gamma_o = -5.5°$, and clearance angle $\alpha_o = 5.5°$) with a silicon carbide abrasive brush (240 mesh). The inserts were brushed to produce seven edge preparations with different values of S_γ and S_α (and, consequently, form factor K) by the proper combination of brush rotational speed and direction, penetration depth, feed speed, and inclination angle [10]. After brushing, the inserts were coated with TiAlN employing physical vapor deposition (PVD).

In addition to the established geometric parameters employed to assess cutting tool edge preparation (r_h, S_γ, S_α, and K), a novel parameter (perimeter ratio P) is proposed. It represents the ratio of the perimeter of the modified cutting edge to the perimeter of a standard honed edge. The perimeter of the modified edge is given by one quarter of the perimeter of an ellipse [17] with axes S_γ and S_α, whereas the perimeter of the standard honed edge is calculated as one quarter of a circumference with radius r_h. Figure 1 shows schematically the cutting edge standard hone radius together with parameters S_γ and S_α.

Equations 1 and 2 present the expressions used to calculate the form factor (K) according to [8] and the proposed perimeter ratio (P), respectively. The values of the geometric parameters tested in this work are presented in Table 1, where it can be seen that the perimeter ratio increases with S_γ and S_α, while the form factor depends on their ratio only. The standard edge hone radius was kept constant ($r_h = 12.4$ μm).

$$K = \frac{S_\gamma}{S_\alpha} \tag{1}$$

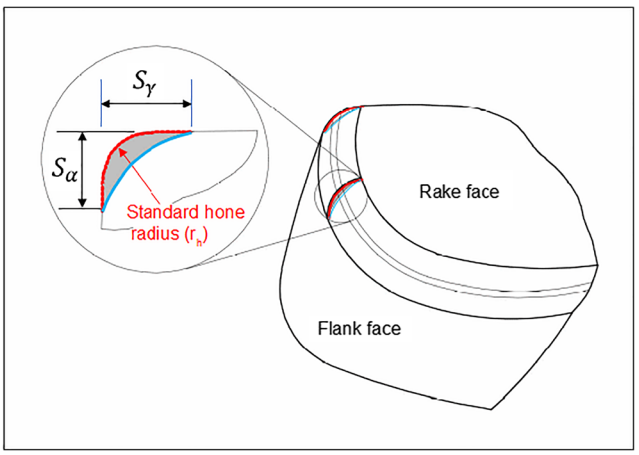

Fig. 1 Fundamental geometric parameters employed in edge preparation

Table 1 Investigated edge preparation parameters

Projection of the hone radius on the rake face S_γ (μm)	Projection of the hone radius on the clearance face S_α (μm)	Form factor K	Perimeter ratio P
30	30	1	2.42
30	60	0.5	3.73
60	30	2	3.73
50	50	1	4.03
50	100	0.5	6.22
100	50	2	6.22
100	100	1	8.06

$$P = \frac{\left[3.(S_\gamma + S_\alpha) - \sqrt{(3.S_\gamma + S_\alpha).(S_\gamma + S_\alpha)}\right]}{\left(\frac{\pi.r_h}{2}\right)} \quad (2)$$

Turning trials were carried out in a computer numerically controlled lathe (maximum rotational speed of 3500 rpm and power of 5.5 kW), and AISI 4140 high-strength, low-alloy (HSLA), low-carbon steel was selected as work material due to its wide range of application. The samples were quenched and tempered to reach two hardness levels: 40 and 50 HRC. The tests were performed dry at a constant cutting condition: cutting speed of 90 m/min, feed rate of 0.15 mm/rev, and depth of cut of 0.5 mm. A Kistler 9121 piezoelectric dynamometer connected to a NI BNC 2110 acquisition board was used to measure the three components (cutting, feed, and passive forces) of the turning force, and a Raytek Marathon MM2ML infrared pyrometer (temperature range from 300 to 1100 °C and a focal diameter of 1.9 mm at a distance of 300 mm from the heat source) was employed to measure the temperature of the chip (T_{chip}); see Fig. 2. DataTemp® Multidrop Rev5.3.1 software was used for recording temperature values. In order to avoid the effect of tool wear, both output variables were measured while turning an axial length of 20 mm, and each experiment was repeated once with a fresh tool cutting edge.

2.2 Analytical modeling

The influence of edge preparation on the three components of the turning force, i.e., cutting force (F_c), feed

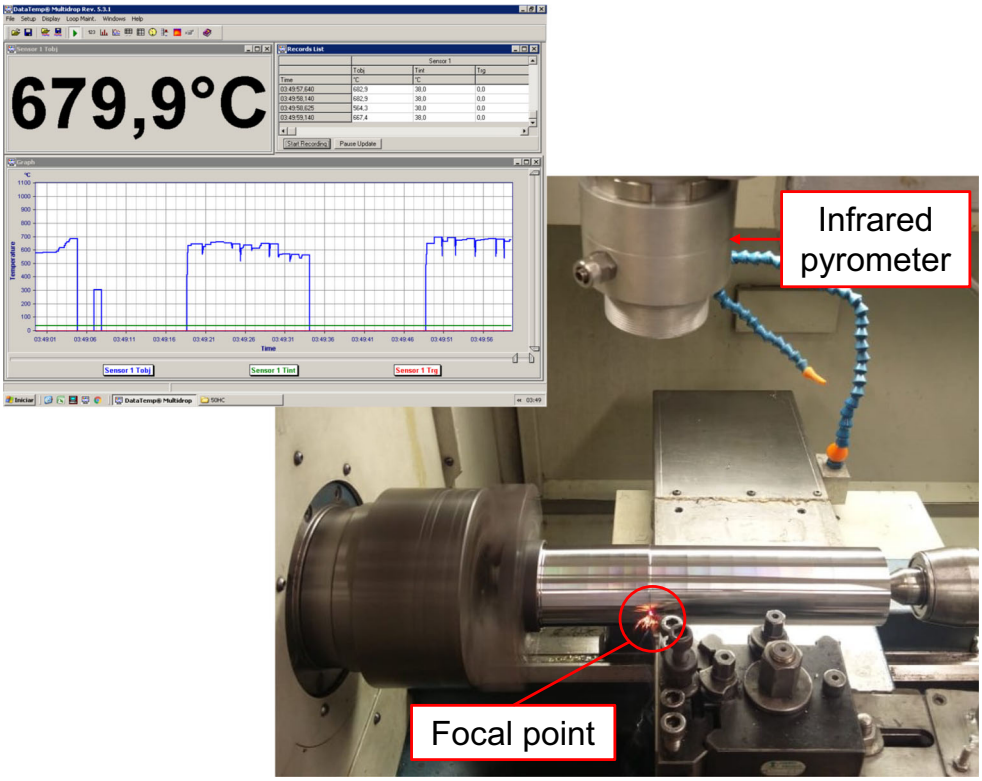

Fig. 2 Experimental setup for chip temperature measurement and software output

Table 2 Coefficients for the determination of the force components when turning hardened AISI 4140 steel using cutting tools with edge preparation

Workpiece hardness	Cutting force for standard edge preparation F_{cstd} (*N*)	a	b	c	d	e	f
40 HRC	325.3	0.931	0.188	0.015	0.042	0.108	−0.-2-28
50 HRC	393.1	0.334	0.382	0.709	0.086	−0.-0-85	−0.-4-35
Workpiece hardness	Feed force for standard edge preparation F_{fstd} (*N*)	a	b	c	d	e	f
40 HRC	144	0.726	0.385	0.104	0.213	0.419	

force (F_f), and passive force (F_p), can be obtained analytically by the product of the corresponding force recorded when using the standard honed edge and the coefficient Ω, as represented in Eq. 3, where F_{prep} stands for the turning force component with a specific edge preparation and F_{std} stands for the force component recorded using the standard honed cutting edge.

The effect of the edge rounding on the rake or clearance face cannot be neglected, since tool-workpiece contact area changes with different values of K. Thus, the coefficient Ω encompasses both the form factor (K) and the perimeter ratio (P). Preliminary attempts indicated that the coefficient Ω did not present a linear relationship with K and P; therefore, the Levenberg-Marquardt algorithm, typically applied to nonlinear models, was used with the aid of a MATLAB routine [18]; see Eq. 4. Table 2 presents the values of the force components recorded using the standard insert (F_{std}) and the coefficients for each workpiece hardness.

$$F_{prep} = \Omega . F_{std} \tag{3}$$

$$\Omega = a + b.K + c.lnP + d.K^2 + e(lnP)^2 + f.K.(lnP) \tag{4}$$

This model is based on the hypothesis that the mechanical load applied during turning with a tailored edge is proportional to the load produced by a standard edge and can be associated with the dependence of the turning force components on the cutting area.

2.3 Finite element modeling

In order to numerically simulate the behavior of the components of the turning force and the temperature both on the chip surface and at the chip-tool interface during hard turning with the application of different cutting edge geometries, Deform 3D software with an updated Lagrangian formulation was used. The workpiece, represented by a circular arc (diameter of 75 mm and angle of 15°), is fixed in all directions, while the insert can move around it with the determined cutting speed; see Fig. 3a. The insert is considered as an elastic body capable of exchanging heat with the workpiece, while the workpiece can exchange heat with the insert and environment and is modeled considering a viscoplastic behavior. Chip separation was obtained by automatic remeshing. This choice is due to the fact that during numerical chip formation, extreme distortions of the elements are observed; i.e., the geometric shape is changed at each time step, thus requiring a new discretization (remeshing). The software Deform 3D performs automatic remeshing for second-order tetrahedral elements. The insert

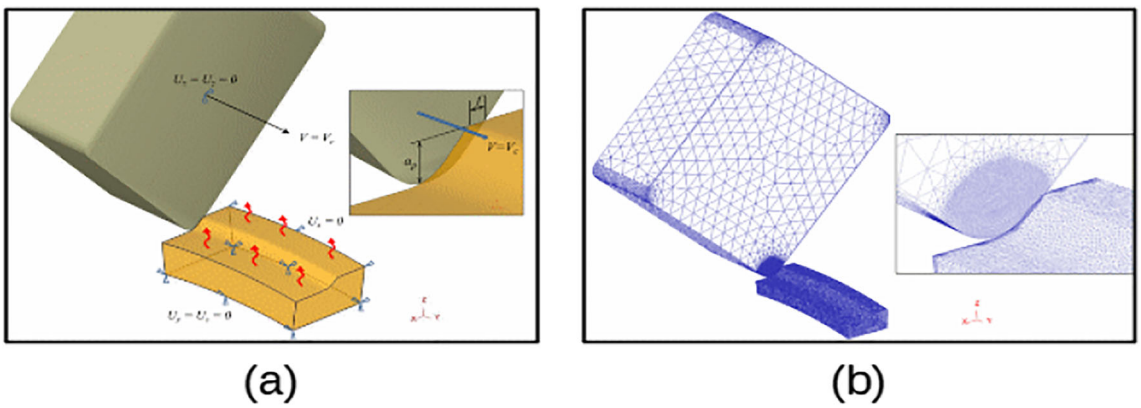

Fig. 3 **a** Geometric model of the tool and workpiece with the boundary conditions and **b** discretization

Table 3 Johnson-Cook constants for AISI 4140 steel

Workpiece hardness	A (MPa)	B (MPa)	n	C	m	$\dot{\varepsilon}_0$ (s^{-1})	T_0 (°C)	T_m (°C)
40 HRC	1155	876.2	0.214	0.0180	1.034	0.001	25	1500
50 HRC	1599	946	0.204	0.0179	0.9586	0.001	25	1500

is discretized with 54,554 elements and the workpiece with 126,819 elements. In order to ensure the applicability of Zorev's model [19] and numerical precision in the contact zone between the insert and the workpiece, it becomes necessary to use elements with minimum size of 0.005 mm (insert) and 0.01 mm (workpiece). In the numerical simulations, elements with 0.001 mm were used to discretize the thickness 0.003 mm of the insert coating. The model discretization can be observed in Fig. 3b.

From the continuum mechanics, each point at the tool-workpiece contact region must satisfy simultaneously (and at any time) the following mechanical and thermal balance equations:

$$div\sigma + f_v = \rho \cdot \ddot{u} \tag{5}$$

$$\lambda \cdot \nabla^2 T - \rho \cdot c_p \cdot T + \dot{q}_v = 0 \tag{6}$$

where σ is the effective stress, f_v is the body force density vector, ρ is the material density, $\ddot{u}$ is the acceleration vector, T is the temperature, λ is the thermal conductivity, c_p is the heat capacity, and $\dot{q}_v$ is the volumetric heat generation in the workpiece.

The flow curve for AISI 4140 steel was obtained through Johnson-Cook constitutive model (Eq. 7), which takes into account the effects of work hardening and thermal softening.

$$\bar{\sigma}(\varepsilon, \dot{\varepsilon}, T) = \underbrace{[A + B \cdot (\bar{\varepsilon}^p)^n]}_{\text{Hardening}} \cdot \underbrace{[1 + C \cdot \ln(\frac{\dot{\bar{\varepsilon}}^p}{\dot{\varepsilon}_0})]}_{\text{Viscosity}} \cdot \underbrace{[1 - (\frac{T - T_0}{T_m - T_0})^m]}_{\text{Softening}} \tag{7}$$

where $\bar{\sigma}$ is the equivalent stress; A, B, C, n, and m are the material parameters; $\bar{\varepsilon}^p$ is the equivalent plastic strain; $\dot{\bar{\varepsilon}}^p$ is the equivalent plastic strain rate; $\dot{\varepsilon}_0$ is the reference plastic strain rate; and T_m and T_0 are, respectively, the material melting temperature and the reference room temperature. The calculation of each parameter (Table 3) followed the recommendations by Johnson and Cook [20].

The mechanical behavior is affected by temperature (softening effect); i.e., the mechanical energy is transformed into internal energy or heat, which results in temperature rise. The heat generated due to this phenomenon is described by Eq. 8, where η_p is the plastic work conversion factor (Taylor-Quinney factor), $\bar{\sigma}$ is the equivalent stress, and $\dot{\bar{\varepsilon}}^p$ is the equivalent plastic strain rate. If the deformation rate is high, heat generation can lead to a steep temperature increase since there is not sufficient time to conduct heat away from the deforming metal; therefore, in this work, $\eta_p = 0.90$ was adopted (if deformation is adiabatic $\eta_p = 1$ [21]).

$$\dot{q}_v = \eta_p \bar{\sigma} : \dot{\bar{\varepsilon}}^p \tag{8}$$

The determination of the thermophysical properties becomes necessary because the thermal exchange between the workpiece and environment and between the workpiece and cutting tool is taken into account in the present work. Figure 4 shows the behavior of the thermal conductivity and specific heat with the increase in the temperature of AISI 4140 steel [21]. According to ASM [23], such variables do not vary significantly within the workpiece hardness range tested.

The friction behavior at the tool-chip interface is described by Zorev's hybrid model (Eq. 9), which assumes the coexistence of adhesion and sliding zones [19]. Under adhesion, the normal friction stress (σ_N) reaches its maximum value on the cutting edge, and the shear friction stress (τ_f) equals the shear stress limit of the workpiece material (τ_{max}). Under sliding, however, the normal friction stress is considerably lower, and friction coefficient $\mu = 0.6$ was employed based on the experimental values of the cutting force components.

$$\tau_f = \begin{cases} \mu.\sigma_N & if \quad \mu.\sigma_N < \tau \quad \text{(sliding zone)} \\ \tau_{max} & if \quad \mu.\sigma_N \geq \tau \quad \text{(adhesion zone)} \end{cases} \tag{9}$$

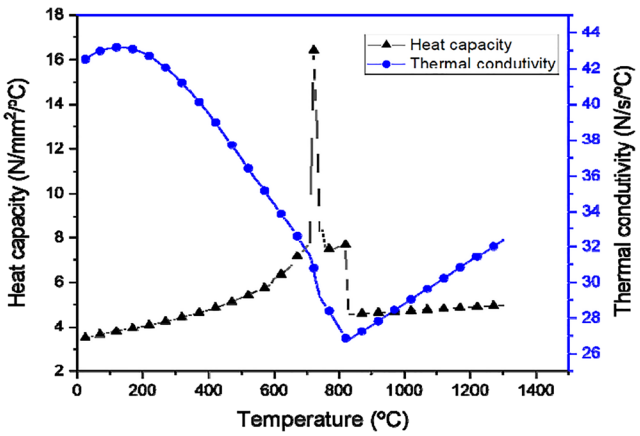

Fig. 4 Thermophysical properties of AISI 4140 steel [22]

The friction between tool and chip also generates heat $\dot{q}_f$, which can be assessed by Eq. 10, where τ_f is the friction stress given by Eq. 9, $\dot{\gamma}$ is the relative sliding velocity, and η_f is the frictional work conversion factor. Assuming that all frictional work is converted into heat, $\eta_f = 1$.

$$\dot{q}_f = \eta_f \cdot \tau_f \cdot \dot{\gamma} \tag{10}$$

In order to determine the heat flux to the cutting insert and workpiece, Eqs. 11 and 12 must be solved.

$$\dot{q}_{\rightarrow \text{insert}} = f_f \cdot \dot{q}_f + h \cdot (T_{\text{int–w}} - T_{\text{int–i}}) \tag{11}$$

Table 4 Relationship between the heat transfer coefficient and pressure [23]

Pressure (MPa)	0	30	180	300	420	600
Heat transfer coefficient h ($kWm^{-2}\ K^{-1}$)	5	18	87	222	410	500

$$\dot{q}_{\rightarrow \text{workpiece}} = \left(1 + f_f\right) \cdot \dot{q}_f - h \cdot (T_{\text{int–w}} - T_{\text{int–i}}) \tag{12}$$

where $\dot{q}_{\rightarrow \text{insert}}$ is the heat flux transmitted to the cutting insert, $\dot{q}_{\rightarrow \text{workpiece}}$ is the heat flux absorbed by the workpiece material

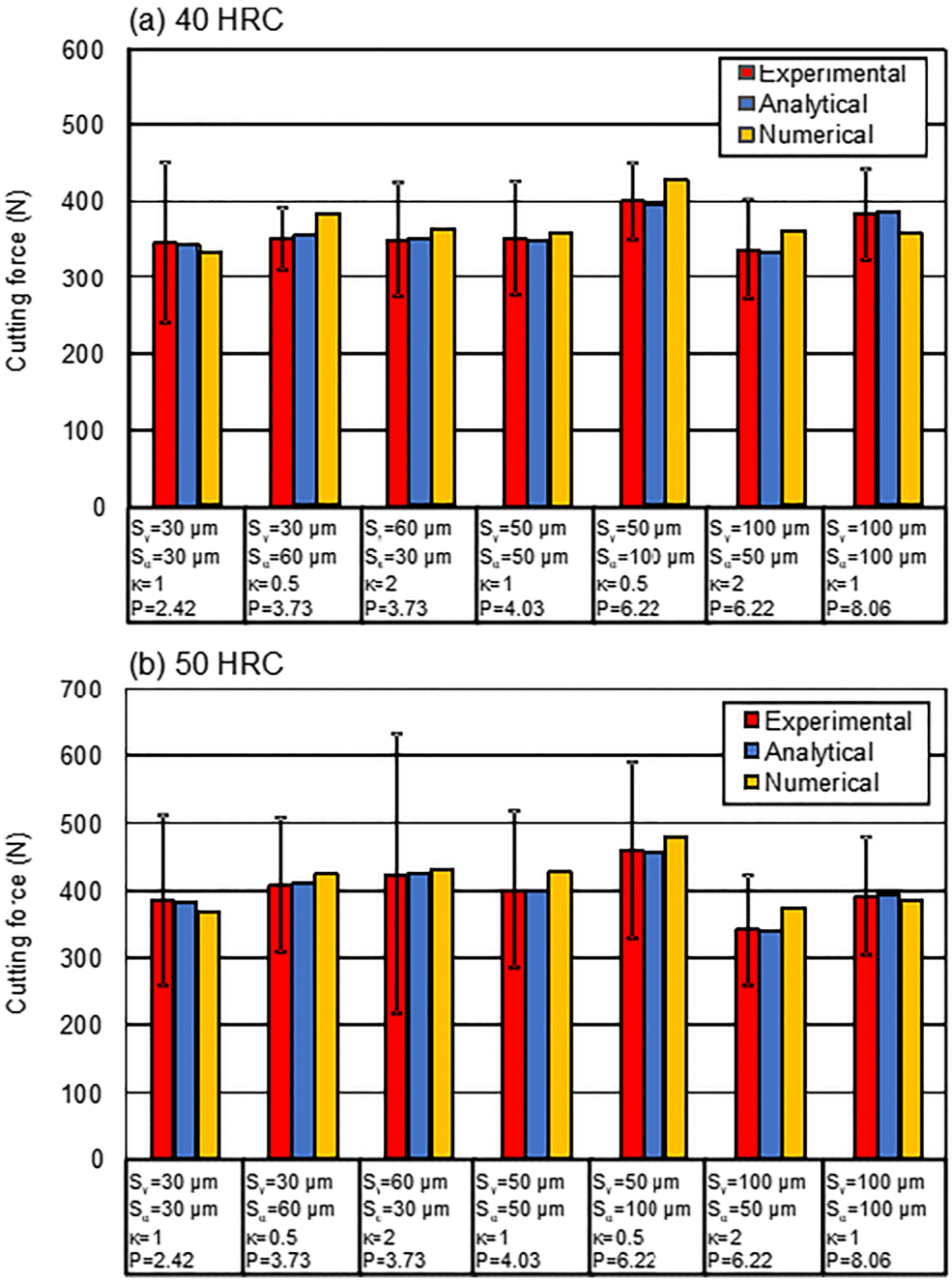

Fig. 5 Influence of cutting edge preparation on the cutting force when turning hardened AISI 4140 steel: **a** 40 HRC and **b** 50 HRC

(calorific energy mainly eliminated through the chip), f_f is the fraction of the friction energy conducted into the insert (heat partition coefficient), h is the interface heat transfer coefficient, while $T_{\text{int-w}}$ and $T_{\text{int-i}}$ are, respectively, the temperatures of the workpiece and insert at the insert-workpiece interface. Considering the work of Rosochowska [24], a heat transfer coefficient (h) based on the pressure at the tool-chip interface was adopted (Table 4).

According to Fig. 3a, only the upper surface of the workpiece exchanges heat with the environment with a convective coefficient of 20 W/m^2 K. An initial temperature of 20 °C was adopted for the insert, workpiece, and environment.

3 Results and discussion

Figure 5 compares the values of the cutting force obtained experimentally, analytically, and numerically for the two workpiece hardness levels and seven different edge preparations tested. Considering the scatter in the experimental data, a satisfactory agreement is noted among the forces obtained using the distinct approaches, and while the values obtained

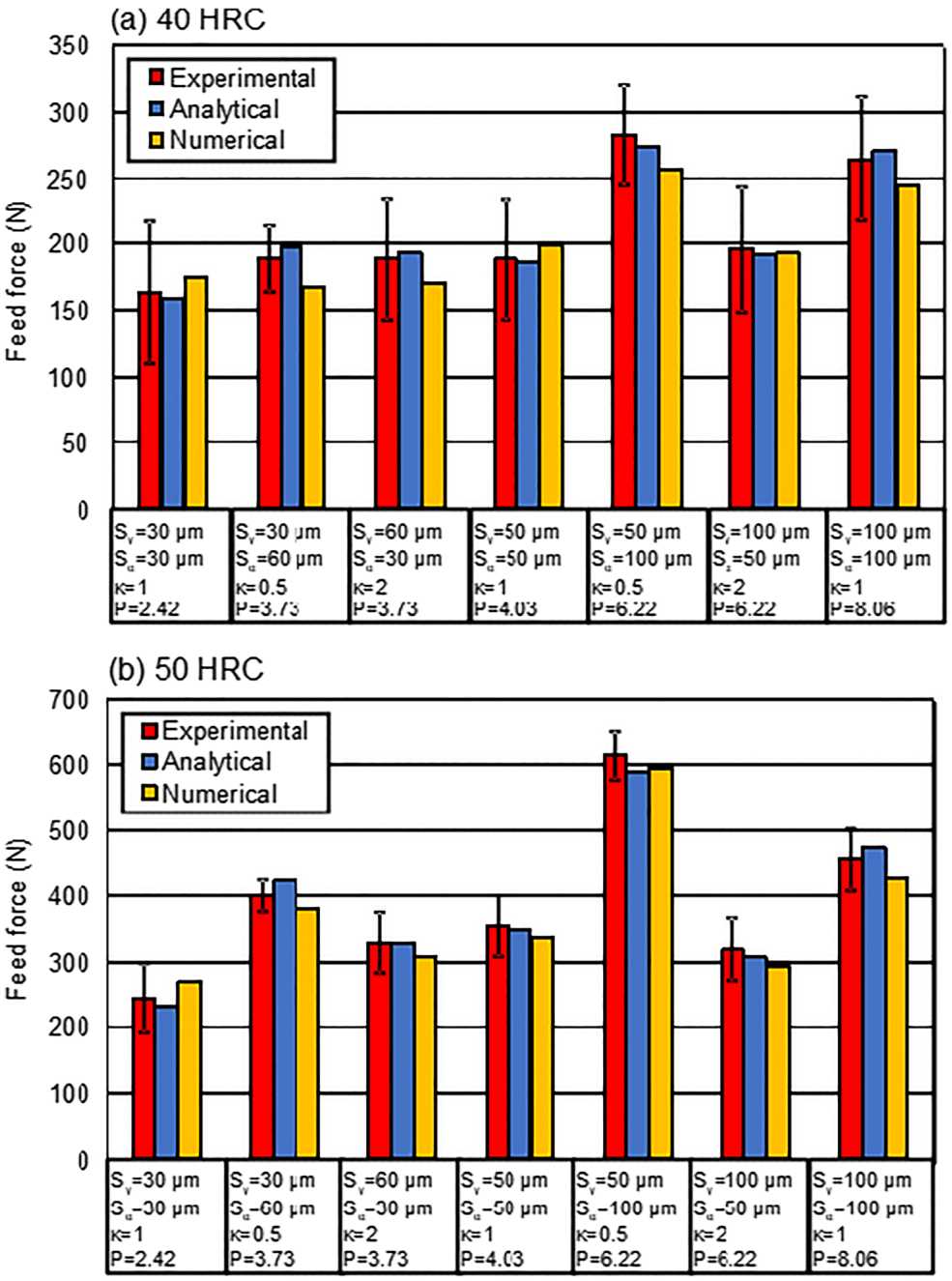

Fig. 6 Influence of cutting edge preparation on the feed force when turning hardened AISI 4140 steel: **a** 40 HRC and **b** 50 HRC

analytically require the experimental force for the standard cutting edge as input, the numerical values are obtained at the expense of computational effort. Moreover, it can be noticed that the different edge preparations tested do not drastically affect the cutting force, which can be explained by the fact that this force component acts normal to the rake face. Comparing Fig. 5a and b, it can be noticed that the elevation of workpiece hardness from 40 to 50 HRC promotes a slight increase in the cutting force due to the higher shear strength of the harder material.

The influence of edge preparation and workpiece hardness on the feed force is given in Fig. 6, where it can be seen that for most edge preparations, the analytical data are closer to the experimental values than the numerical values. According to Haddag et al. [25], this may have occurred owing to the fact that the tool path is considered circular in the numerical simulation, while in the actual process, it performs a helical course. The different force amplitudes show the significant and distinct effects of the form factor and the perimeter ratio on feed force. Keeping the form factor constant, a noticeable elevation of this force component can be obtained by increasing the perimeter ratio, while for a constant and high perimeter ratio ($P = 6.22$), the force tends to be higher for lower form factors. As can be seen in Fig. 1, the larger the value of S_α, the larger the contact area on the clearance face, whereas the larger the value of S_γ, the more negative the effective rake angle in

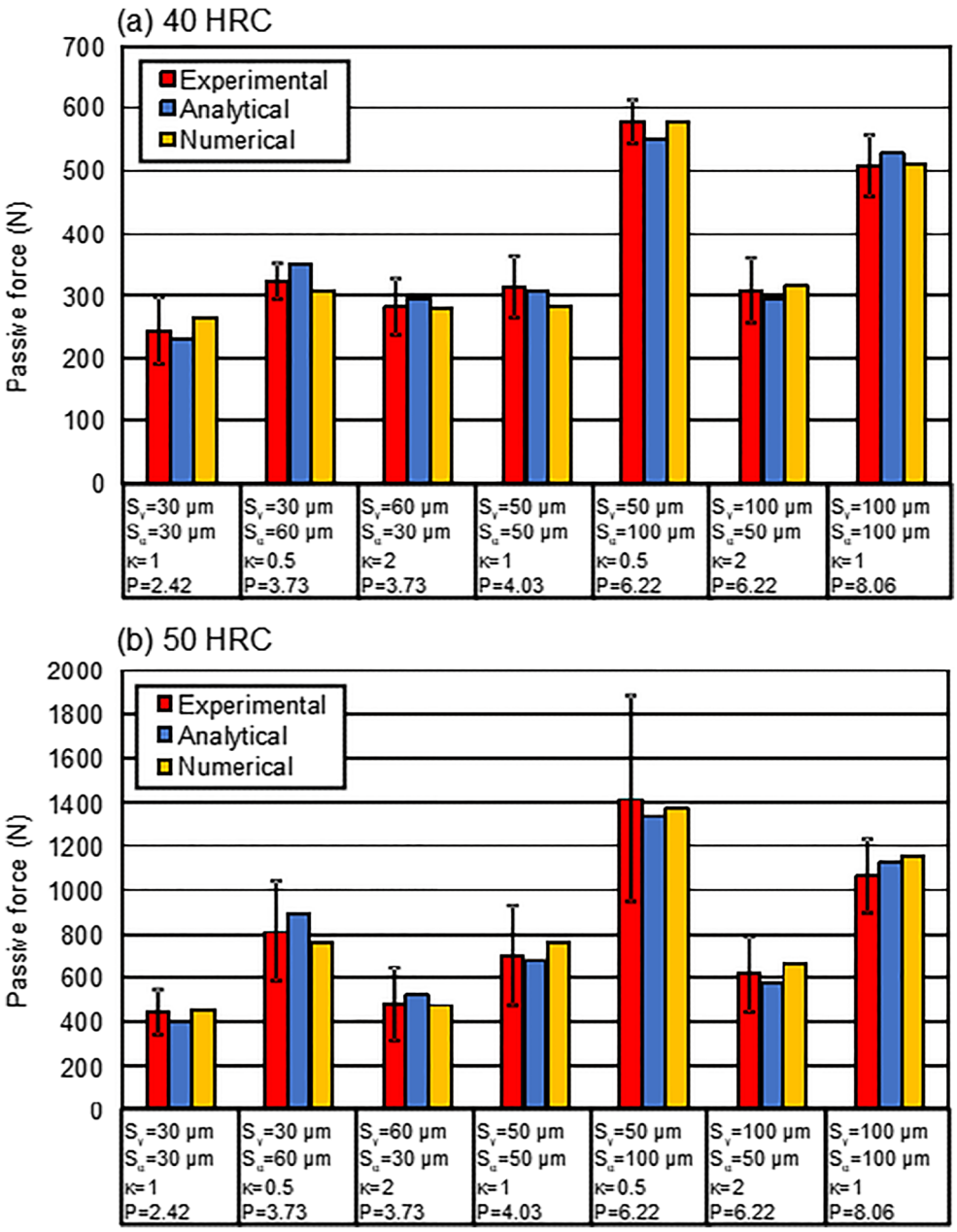

Fig. 7 Influence of cutting edge preparation on the passive force when turning hardened AISI 4140 steel: **a** 40 HRC and **b** 50 HRC

chip formation zone. These two factors are responsible for the elevation of the feed force. In contrast, when the perimeter ratio is low, the tool becomes sharper for the applied chip thickness, and the form factor, mainly responsible for alterations in the effective rake angle, has its influence reduced. Additionally, the elevation of workpiece hardness from 40 HRC (Fig. 6a) to 50 HRC (Fig. 6b) represents, in most cases, a twofold increase in the feed force due to the elevation of the shear strength of the work material.

A trend similar to that observed for the feed force (Fig. 6) is noted for the passive force; see Fig. 7; i.e., the passive force increases with the perimeter ratio (P), but more markedly with S_α to reach its maximum when $S_\alpha = 100$ μm. In contrast, the lowest passive force is recorded when $S_\gamma = S_\alpha = 30$ μm. Nevertheless, the numerical values of the passive force are closer to those obtained analytically. As far as the influence of workpiece hardness is concerned, the elevation from 40 HRC (Fig. 7a) to 50 HRC (Fig. 7b) promotes a remarkable increase in the passive force owing to the fact that a cutting edge angle (χ_r) of 45° was used, thus increasing the contact area in the direction normal to the passive force. Due to the fact that the depth of cut ($a_p = 0.5$ mm) is smaller than the cutting tool nose radius ($r_\varepsilon = 0.8$ mm), the largest part of the resultant force is projected on the reference plane. This explains the highest values and sensitivity of the passive force to changes in edge geometry, followed by the feed force. An increase in the contact area between tool and workpiece reduces the sharpness of the former and makes harder for the tool to penetrate the work material, as well as intensifies chip deformation, increases friction, and leads to an increase in such force components.

Figure 8 presents selected results from the numerical simulation showing the temperature distribution on the top of the chip (view of the reference plane) for different edge preparations and workpiece hardness values and the corresponding values of the temperature of the chip (T_{chip}), to be compared with the experimental values recorded with the infrared pyrometer. It can be noted that the highest chip temperatures are obtained at some distance from the cutting edge associated with the feed rate employed and where adhesion is expected to be more intense. Moreover, Fig. 8 allows a qualitative analysis of the temperature distribution in the chip, not feasible with the infrared pyrometer, which measures the average temperature within a focal diameter of 1.9 mm. It can be seen that, additionally to the expected increase in chip temperature with work material hardness, appreciable changes in the temperature at the top of the chip are obtained with the numerical simulation, thus indicating that the proper and still positioning of the infrared pyrometer is crucial for obtaining reliable experimental results.

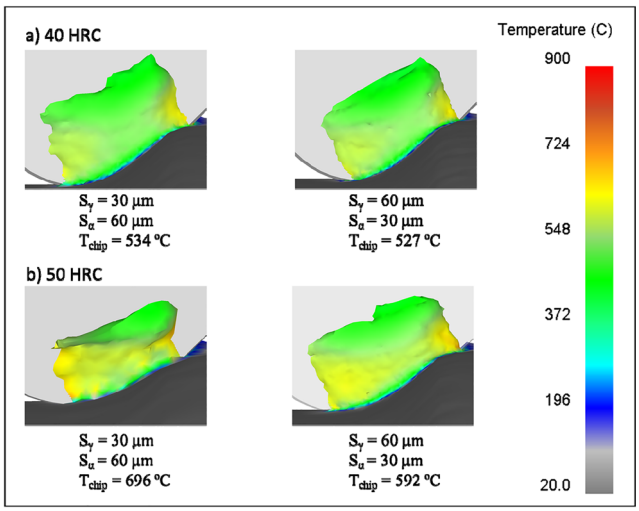

Fig. 8 Temperature distribution on the top of the chips obtained by numerical modeling when turning hardened AISI 4140 steel with selected edge preparations: **a** 40 HRC and **b** 50 HRC

Figure 9 presents the experimental and numerical temperatures of the chip together with the highest temperature at the tool-chip interface for both workpiece hardness values and different edge preparations. In contrast with the feed and passive force results, it can be noted that changes in edge preparation do not contribute significantly to variations in the chip and interface temperatures, and a clear trend cannot be identified. In terms of the cutting force, these results are consistent, since this is the main responsible for heat generation during the process, which is mainly transferred to the chip. Considering AISI 4140 steel hardened to 40 HRC (Fig. 9a), the largest difference between the experimental and numerical chip temperatures is 5.9% ($S_\gamma = 100$ μm and $S_\alpha = 50$ μm), while for AISI 4140 steel hardened to 50 HRC (Fig. 9b), the largest difference is 3.8% ($S_\gamma = 30$ μm and $S_\alpha = 60$ μm). Additionally, when Fig. 9a is compared with Fig. 9b, one can note that the elevation of workpiece hardness from 40 to 50 HRC results in an increase of 98.9 °C in the average experimental chip temperature and 97.9 °C in the average numerical chip temperature, thus validating the proposed numerical model.

In order to compute the effective stress exerted on the tool, the insert was modeled as an elastic object, and the effective stress distribution on the insert for selected microgeometries can be seen in Fig. 10. It can be noted that the highest effective stresses were obtained for the hardest work material (50 HRC) and that a reduction in S_α resulted in a decrease in stress intensity (708 MPa for the steel hardened to 40 HRC and 1010 MPa for 50 HRC), as well as better stress distribution, thus probably leading to superior cutting tool performance (longer tool life).

4 Conclusions

Analytical and numerical analyses of the turning force components and numerical analysis of the cutting temperature

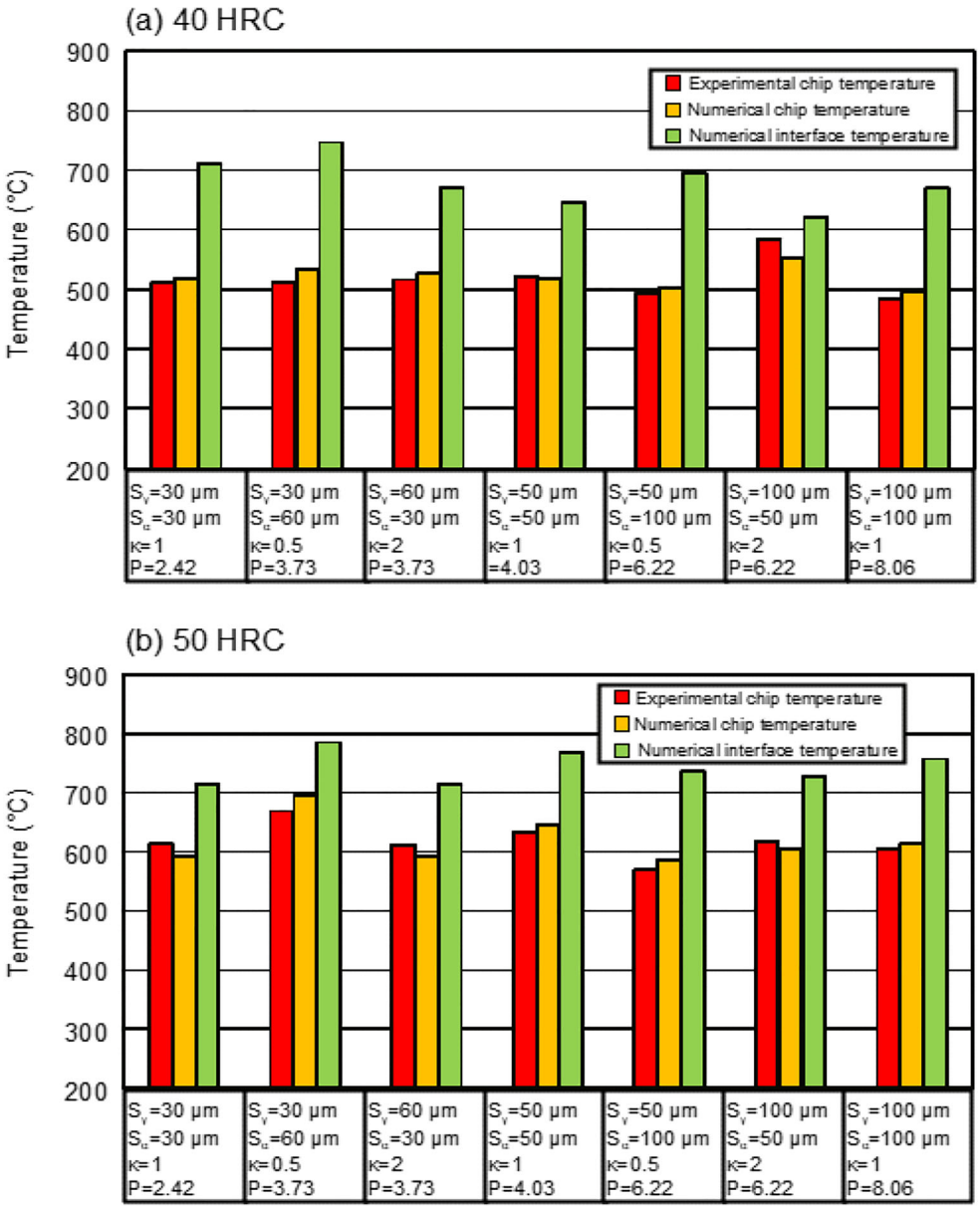

Fig. 9 Influence of cutting edge preparation on the chip and interface temperatures when turning hardened AISI 4140 steel: **a** 40 HRC and **b** 50 HRC

were performed after hard turning of AISI 4140 steel (40 and 50 HRC) with coated tungsten carbide inserts with different cutting edge preparations, and the following conclusion were obtained:

- On the one hand, the analytical modeling was capable to satisfactorily predict the variation of the force components with edge preparation using as input the value of the corresponding experimental forces for a standard honed cutting edge. On the other hand, the numerical modeling was successfully applied to predict the components of the resultant force at the expense of a higher computational effort.
- The proposed geometric parameter (perimeter ratio P) and the projection of the hone radius on the clearance face (S_α) affected the values of the feed and passive components of the turning force, which reached their highest values for $S_\alpha = 100$ μm and $P = 6.22$. In contrast, changes in the projection of the hone radius on the rake face (S_γ) and in the form factor (K) could not be associated with alterations in the feed and passive forces. The cutting force was not marked by the geometric parameters of the cutting edge, probably due to the fact that it acts on the rake face and normal to the cutting edge; therefore, seizure and sliding conditions in a much larger area (tool-chip interface) will overwhelm the influence of cutting edge geometry on the cutting force.
- The numerical approach was not capable to detect the effect of the geometric parameters neither on the chip temperature nor on the tool-chip interface temperature. This result may be associated with the temperature

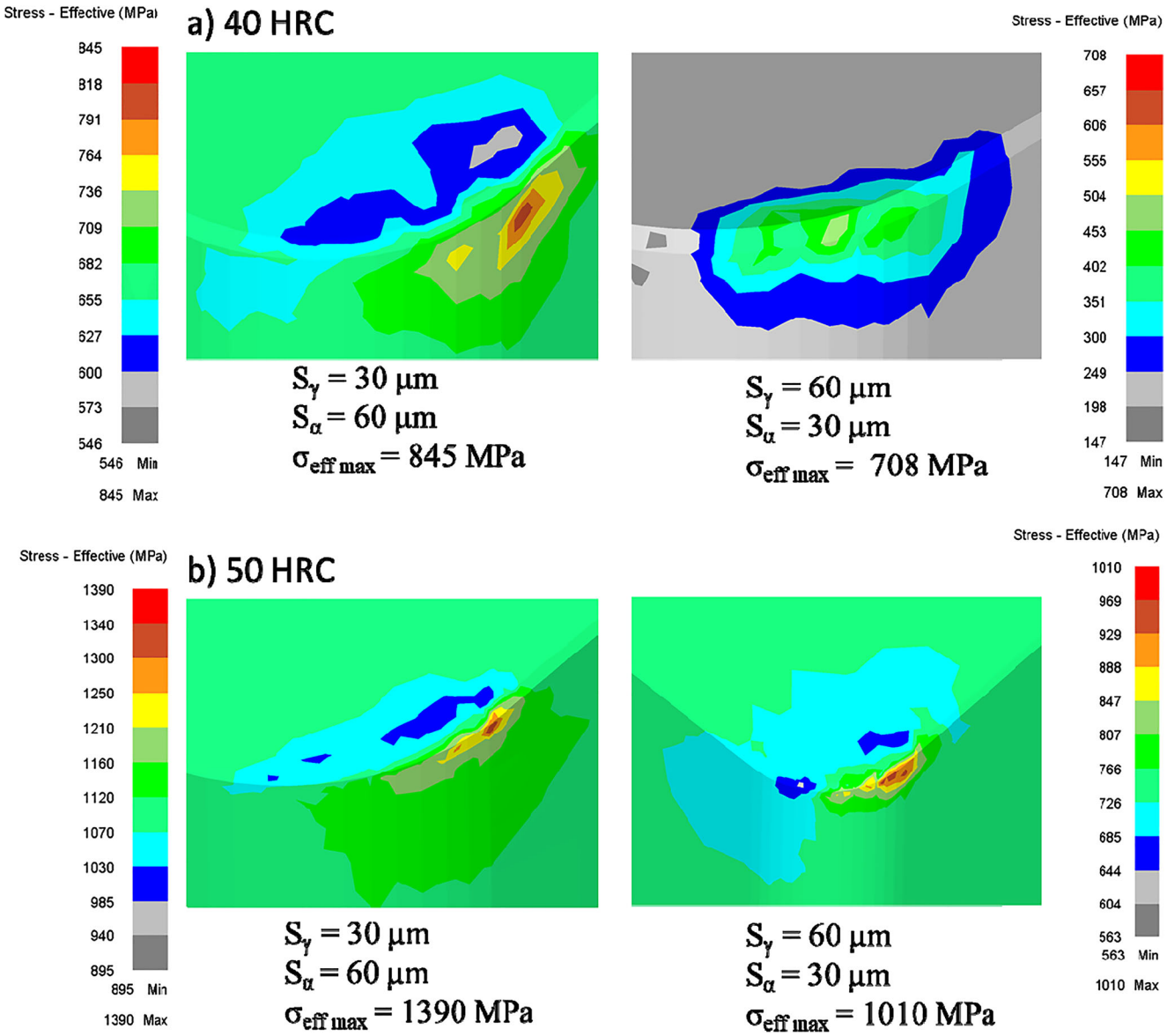

Fig. 10 Stress distribution on the inserts simulated for turning hardened AISI 4140 steel with selected edge preparations: **a** 40 HRC and **b** 50 HRC

measurement technique employed (infrared pyrometry), which detected the outer temperature of the chip, i.e., the temperature in a region at least 0.15 mm away from the heat generation zone. Secondly, alterations in the chip and interface temperatures are closely related to the power required by the operation, which is directly dependent on the cutting force (not affected by the geometric parameters).

- The numerical results showed that the reduction in the S_α parameter promoted a decrease in the effective stress values and its better distribution. Consequently, cutting tool performance is expected to improve, especially tool life.

Acknowledgments The authors would like to thank the Brazilian-German Collaborative Research Initiative on Manufacturing Technology (CAPES/DFG BRAGECRIM 029/14) supported by the Coordination for the Improvement of Higher Education Personnel (Brazil) and the German Research Foundation.

Authors' contributions Carlos E.H. Ventura was responsible for the experimental design and cutting edge preparation, Frederico C. Magalhães was responsible for the analytical and numerical modeling, and Alexandre M. Abrão and Bernd Breidenstein were responsible for the experimental data collection, as well as for manuscript preparation and revision together with Berend Denkena.

Funding This work was funded by the Brazilian-German Collaborative Research Initiative on Manufacturing Technology supported by the Coordination for the Improvement of Higher Education Personnel (Brazil) and the German Research Foundation (Grant CAPES/DFG BRAGECRIM 029/14).

Data availability Not available.

Compliance with ethical standards

Conflict of interest The authors declare that they have no competing interests.

Ethical approval Not applicable.

Consent to participate Not applicable.

Consent for publication Not applicable.

Code availability Not applicable.

References

1. Lima JG, Ávila RF, Abrão AM (2007) Turning of hardened AISI 4340 steel using coated carbide inserts. Proc IMechE B J Eng Manuf 221:1359–1366
2. Matsumoto Y, Barash MM, Liu CR (1986) Effect of hardness on the surface integrity of AISI 4340 steel. Trans ASME J Eng Ind 112:245–252
3. Bergmann B, Grove T (2018) Basic principles for the design of cutting edge roundings. CIRP Ann Manuf Technol 67:73–78
4. Aurich JC, Zimmermann M, Leitz L (2011) The preparation of cutting edges using a marking laser. Prod Eng Res Dev 5:17–24
5. Karpuschewski B, Byelyayev O, Maiboroda VS (2009) Magneto-abrasive machining for the mechanical preparation of high-speed steel twist drills. CIRP Ann Manuf Technol 58:295–298
6. Yussefian NZ, Koshy P, Buchholz S, Klocke F (2010) Electro-erosion edge honing of cutting tools. CIRP Ann Manuf Technol 59:215–218
7. Denkena B, Köhler J, Ventura CEH (2013) Customized cutting edge preparation by means of grinding. Precis Eng 37:590–598
8. Denkena B, Lucas A, Bassett E (2011) Effects of the cutting edge microgeometry on tool wear and its thermomechanical load. CIRP Ann Manuf Technol 60:73–76
9. Zhao T, Zhou JM, Bushlya V, Stahl JE (2017) Effect of cutting edge radius on surface roughness and tool wear in hard turning of AISI 52100 steel. Int J Manuf Technol 91:3611–3618
10. Ventura CEH, Chaves HS, Campos Rubio JC, Abrão AM, Denkena B, Breidenstein B (2017) The influence of the cutting tool microgeometry on the machinability of hardened AISI 4140 steel. Int J Adv Manuf Technol 90:2557–2565
11. Khan SA, Umar M, Saleem MQ, Mufti NA, Raza SF (2018) Experimental investigations on wiper inserts' edge preparation, workpiece hardness and operating parameters in hard turning of AISI D2 steel. J Manuf Process 34:187–196
12. Souza DJA, Weingaertner WL, Schroeter RB, Teixeira CR (2014) Influence of the cutting edge micro-geometry of PCBN tools on the flank wear in orthogonal quenched and tempered turning M2 steel. J Braz Soc Mech Sci Eng 36:763–774
13. Tiffe M, Assmuth R, Biermann D (2019) Investigation on cutting edge preparation and FEM assisted optimization of the cutting edge micro shape for machining of nickel-base alloy. Prod Eng 13:459–467
14. Liao T, Jiang F, Yan L, Cheng X (2017) Optimizing the geometric parameters of cutting edge for finishing machining of Fe-Cr-Ni stainless steel. Int J Manuf Technol 88:2061–2073
15. Yen Y-C, Jain A, Altan T (2004) A finite element analysis of orthogonal machining using different tool edge geometries. J Mater Process Technol 146:72–81
16. Hua J, Umbrello D, Shivpuri R (2006) Investigation of cutting conditions and cutting edge preparations for enhanced compressive subsurface residual stress in the hard turning of bearing steel. J Mater Process Technol 171:180–187
17. Berndt B (1998) Ramanujan's Notebooks, vol 3. Springer, New York
18. Madsen K, Nielsen HB, Tingleff O (2004) Methods for non-linear least squares problems, 2nd edn. Informatics and Mathematical Modeling, Technical University of Denmark, Copenhagen
19. Zorev NN (1966) Metal cutting mechanics, 1st edn. Pergamon Press Ltd., Oxford
20. Johnson GR, Cook WH (1983) A constitutive model and data for metals subjected to large strains, high strain rates and high temperatures. In: Proc. of the 7th Int. Symp. Ballistics, Hague, Netherlands, pp 541–547
21. Hosford WF, Caddell RM (2011) Metal forming – mechanics and metallurgy, 4th edn. Cambridge University Press, New York
22. JAHM SOFTWARE. MPDB (Material Properties Database). https://www.jahm.com/. Accessed in 03/07/2020
23. ASM HANDBOOK (2013) Steel heat treating fundamentals and processes, vol 4A. ASM International, Materials Park
24. Rosochowska M, Balendra R, Chodnikiewicz K (2003) Measurements of thermal contact conductance. J Mater Process Technol 35:204–210
25. Haddag B, Kagnaya T, Nouari M (2012) A new heat transfer analysis in machining based on two steps of 3D finite element modeling and experimental validation. Heat Mass Transf 49:129–145